The Vertical Structure of New England Coastal Fronts

JOHN W. NIELSEN* AND PETER P. NEILLEY

Center for Meteorology and Physical Oceanography, Massachusetts Institute of Technology, Cambridge, Massachusetts

(Manuscript received 21 August 1989, in final form 5 March 1990)

ABSTRACT

Aircraft data from the New England Winter Storms Experiment (NEWSEX) are used to examine the vertical structure of four New England coastal fronts. The aircraft made multiple passes at varying elevations through the coastal fronts. The observations were projected onto cross sections normal to the coastal fronts using frontal orientations determined from surface analyses and frontal velocities determined from a least-squares fit to multiple frontal penetrations.

The frontal zones were found to be roughly 200 m wide, rising sharply from the ground to a height of 150 m to 400 m over distances of 0.5 to 2.5 km before leveling off and rising gradually toward the mountains. The underlying pools of cold air were similar in form and flow patterns to cold-air damming structures observed elsewhere along the East Coast. The coastal fronts formed the leading edges of the cold pools. Air on the warm side of the fronts was neutrally stratified, having been recently heated by the warm Gulf of Maine. This warm air attained vertical velocities of up to 2.5 m s^{-1} as it rose over the coastal fronts and accelerated toward the mountains, and evidence is found for direct precipitation enhancements by this updraft.

The coastal fronts possessed characteristics of atmospheric density currents, with a low-level inflow within the cold air toward the head and turbulent mixing behind the head. Because the fronts were quasi-stationary and were located in neutrally stratified environments, a direct comparison is made with theoretical predictions of inviscid density current behavior. The observed frontal velocities relative to the warm air were found to be within about 1 m s^{-1} of the velocities predicted by inviscid density current theory.

Richardson numbers are estimated at the leading edge of the coastal front and along the frontal inversion beyond the region of rapid mixing behind the head. The Richardson numbers are found to be consistent with Kelvin–Helmholtz instability originating at the leading edge of the coastal front.

1. Introduction

Most case studies of New England coastal fronts (e.g., Bosart et al. 1972; Bosart 1975; Nielsen 1989) have been limited to the horizontal structure of coastal fronts, partly by design and partly because of observational limitations. These studies have described the surface weather patterns associated with New England coastal fronts and have discussed the causes of coastal frontogenesis in detail. Most New England coastal fronts form along the Maine–New Hampshire–eastern Massachusetts coastline as an anticyclone to the north moves eastward and winds become onshore. The frontal circulation is initially driven by differential heating from the relatively warm sea surface, often in combination with nocturnal cooling over land. The fronts tend to remain quasi-stationary and can develop temperature differences of 10°C or more across a frontal zone less than 1 km wide (Sanders 1983). The fronts can act as mesoscale modulators of large-scale precipitation, with local enhancement of precipitation behind the front (Marks and Austin 1979), and the fronts themselves often separate regions of frozen and nonfrozen precipitation.

The vertical structure of New England coastal fronts has been less extensively studied. McCarthy (1977) examined the structure of the lower troposphere for several coastal front events using rawinsonde observations, but his cross sections were able to incorporate only a single sounding between the coastal front and the mountains. A more detailed representation of the possible vertical structure of coastal fronts was produced by Ballentine (1980), whose numerical simulation of coastal frontogenesis suggested that the coastal front extends back toward the mountains as a cold-air damming inversion (cf. Forbes et al. 1987; Bell and Bosart 1988). Coastal frontogenesis and cold-air damming tend to occur together, particularly in the Carolinas (e.g., Bosart 1981), where the damming effects are often more intense than in New England.

In this study, we use aircraft observations to determine the vertical structure of four New England coastal fronts. The observing systems and analysis techniques are described in section 2. In section 3, cross sections through the fronts are presented, and the observed structures are compared to other atmospheric fronts and cold-air damming situations. In section 4, the coastal fronts are compared quantitatively to laboratory

* Present affiliation: Department of Atmospheric Science, State University of New York at Albany.

Corresponding author address: Dr. John W. Nielsen, ES 229, Department of Atmospheric Sciences, SUNY, Albany, NY 12222.

and theoretical density currents. The existence of shear instability along the frontal interface is investigated in section 5. Concluding remarks are contained in section 6.

2. Observations and analysis techniques

The data for this study were collected during the New England Winter Storms Experiment (NEWSEX). The NCAR Queen-Air instrumented aircraft made multiple passes through coastal fronts on 10 January 1983 and 15 January 1983 (referred to below as the 10 Jan and 15 Jan fronts), and the NCAR King-Air made passes through fronts on 4 December 1983 and 12 December 1983 (the 4 Dec and 12 Dec fronts). Surface analyses of the four coastal fronts, indicating the timing and location of the aircraft observations, are shown in Fig. 1. According to the categorization of Nielsen (1989), the 15 Jan and 4 Dec fronts were Type A coastal fronts, while the 10 Jan and 12 Dec fronts were Type B coastal fronts. Both types of fronts form near the diabatic heating discontinuity at the coastline, with Type A fronts triggered by the ambient winds becoming onshore and Type B fronts triggered by nocturnal cooling over land. A case study of the formation of the 4 Dec front may be found in Nielsen (1989).

Both aircraft were equipped to measure state, dynamical, and microphysical parameters, including temperature, dewpoint, three-dimensional winds, and cloud and precipitation particle distributions. The aircraft were flown at varying altitudes in a series of four to seven passes through and one to five passes over the coastal fronts. The altitudes ranged from 20 m (over water) to 3000 m. Each complete set of passes took from 1.5 to 2 hours to complete. The data sampling rate of once per second produced a typical horizontal data resolution of 65 m with the Queen-Air and 85 m with the King-Air. The flight paths also included ascents and descents through the coastal front inversions and overlying warm frontal inversions.

The data from each set of passes were projected onto an x–z plane perpendicular to the coastal front, using frontal orientations determined from surface analyses. Based on the limited range of frontal orientations consistent with the surface observations, we estimate the orientations to be accurate to within 4°. This 4° uncertainty in frontal orientation affects the separation of horizontal wind into components parallel to and normal to the front, resulting in, for example, errors of up to 0.4 m s^{-1} in the component of wind toward the front in the warm air.

Data within 5 km (warm side) or 15 km (cold side) of the surface frontal position were placed in a moving front-relative coordinate system, using mean frontal velocities determined from aircraft data by a method described in appendix A. Data outside the neighborhood of the front were kept fixed relative to the ground, in order to retain the structure of flow variations caused by the underlying orography.

Successive aircraft passes at similar levels provided a check on the steady-state nature of the coastal fronts. Winds within the warm and cold air varied little, but temperatures rose steadily during the periods of observation. To remove the temperature trends, linear corrections were applied to all temperatures based on the observed changes of temperature in the warm air near the front. Within the frontal inversions, successive passes were often locally inconsistent, suggesting rapidly varying small-scale structure.

In constructing cross sections composed of aircraft observations collected over a period of 1–2 hours, it was desirable to eliminate small-scale features that could not be adequately observed by successive aircraft passes. For this reason, the subjective analyses depicted in Figs. 2–4 (below) were performed on 30-second averages of wind and temperature, corresponding to horizontal averaging over 2 to 3 km. The unsmoothed 1-second data were used to determine the width of the leading edges of the coastal fronts. High resolution data were also used during rapid changes in aircraft altitude to determine lapse rate structure.

3. Analyses of vertical structure

a. Overview of frontal cross sections

Figures 2, 3 and 4 are cross section analyses (with vertical exaggeration of 50:1) of potential temperature, front-normal wind, and front-parallel wind. The front-normal wind is defined as the observed wind component normal to the front minus the frontal velocity, i.e. the motion of air relative to the front. The front is seen as a sharp transition zone of front-normal wind and temperature that intersects the ground near $x = 0$ km, rises steeply to a height of 150 m to 400 m, and then slopes gradually back over the coastal plain and the first inland hills.

The same overall pattern of temperature and front-normal wind is repeated in each of the four coastal fronts. In contrast, the front-parallel winds (Fig. 4) show large case-to-case variations, especially in the vicinity of the surface fronts. The 10 Jan front has a front-parallel wind discontinuity similar in form to the front-normal wind and temperature discontinuities. The 10 Jan front was also the only front in which the warm air had a southwesterly (positive front-parallel) component. With the other three fronts, northeasterly (negative) winds are found throughout. A nearly vertical, narrow region of reduced northeasterly flow is present at the leading edges of these three fronts. Trajectory analyses indicate that the air parcels within these narrow bands originated near the ground, where their horizontal velocities had been reduced by friction, and were then advected upward along the frontal interface.

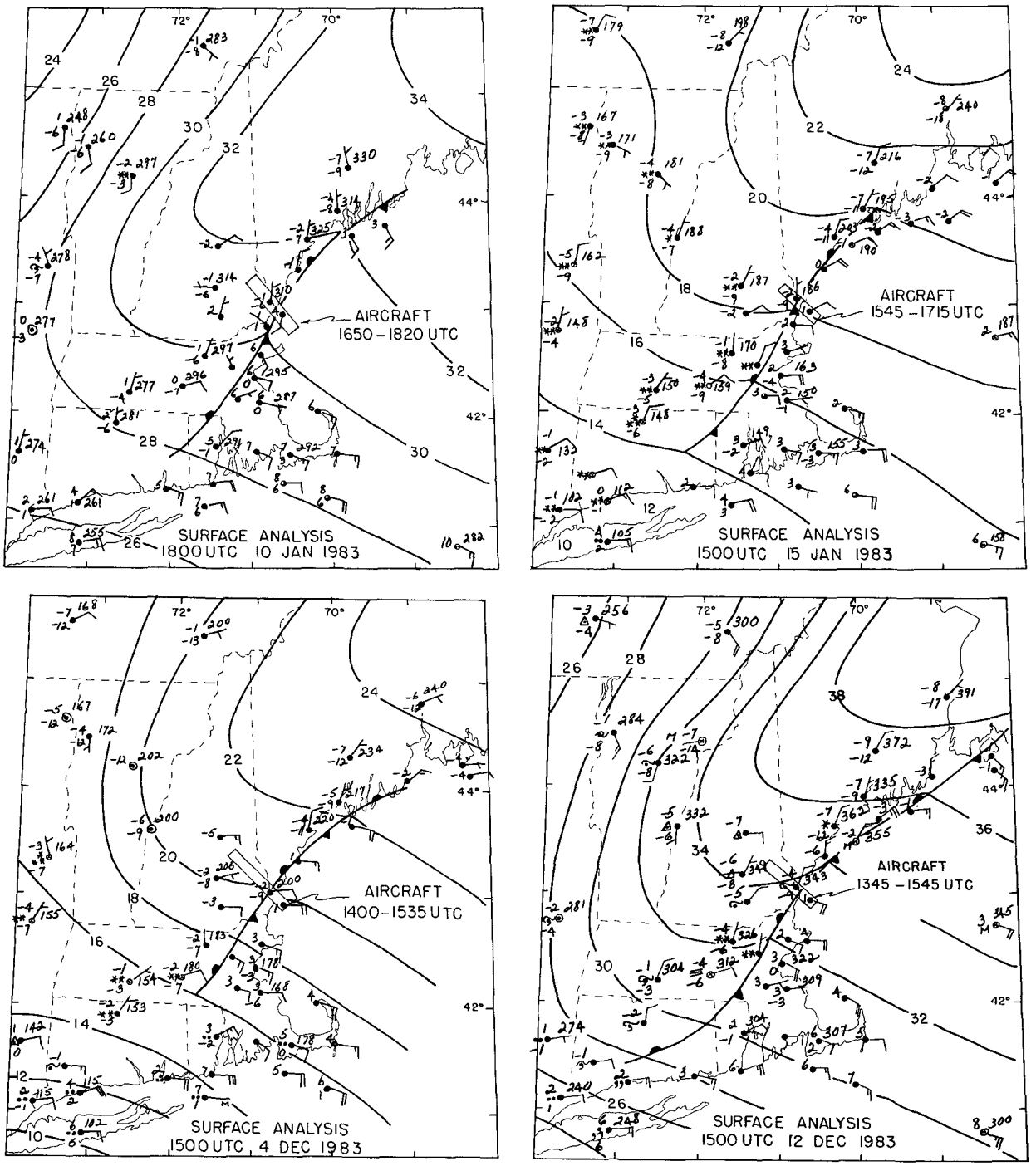

FIG. 1. Surface analyses of the four coastal fronts examined in this study, showing location and time of aircraft observations. Sea level pressure is subjectively analyzed with a 2 mb contour interval, and the positions of the coastal fronts are indicated by the symbol for a stationary front. Selected hourly and Coast Guard station observations are plotted, showing sky cover, wind (long barb equals 5 m s^{-1}, short barb equals 2.5 m s^{-1}), temperature (°C), weather (standard symbols), dewpoint (°C), and sea level pressure (tenths of mb, leading digits dropped) in the standard station model format.

b. Cold-air damming structure

Farther behind the fronts, at ranges of 5 to 50 km, the parallel wind structure closely resembles the cold-air damming wind structure analyzed by Bell and Bosart (1988). They demonstrated that the northeasterly low-level cold air wind maximum is generated by the large-scale mountain-parallel pressure gradient. As the

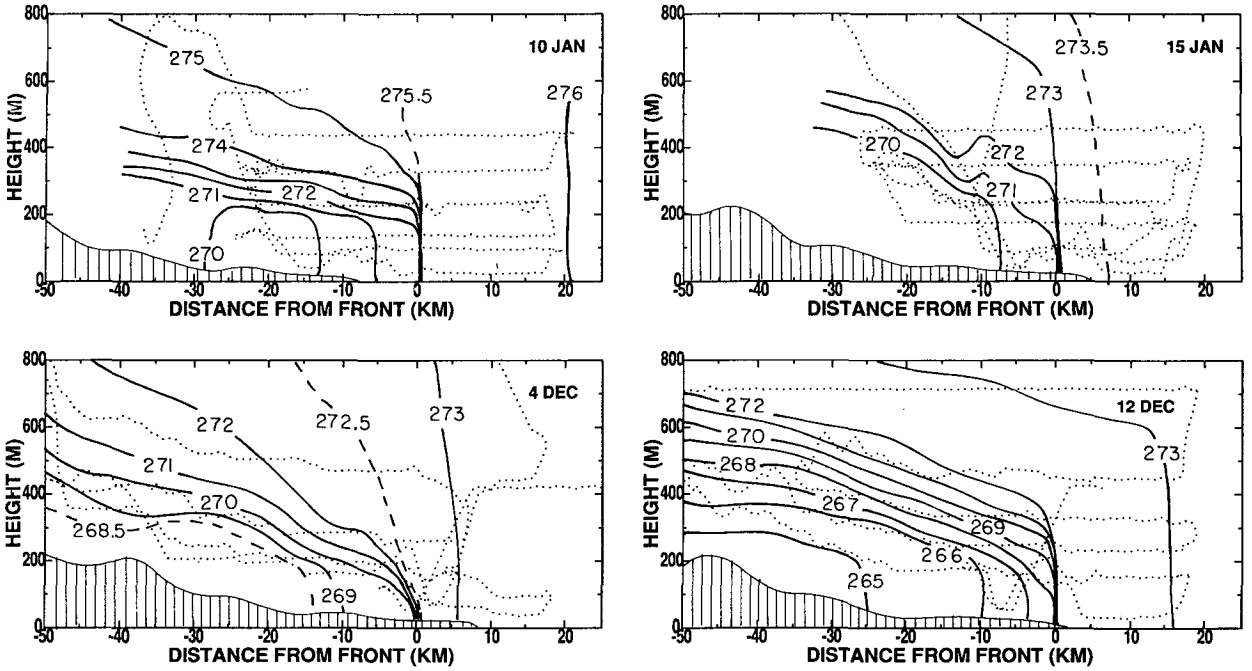

FIG. 2. Cross sections normal to the coastal fronts of potential temperature (K), subjectively analyzed. See text for description of method of construction. Dotted lines indicate path of aircraft. Surface topography is shown by vertical hatching, with the coastline located at the right-hand edge of the hatched region. Aspect ratio is 50:1.

Coriolis force attempts to turn the flow to the right, the air is blocked by the mountains, creating a sloping inversion whose associated pressure gradient balances the Coriolis force. The balance of forces in the along-front direction is between the large-scale gradient and surface drag. In the limit of a discontinuity at the inversion, the orography, ambient pressure gradient, friction, and frontal temperature difference completely

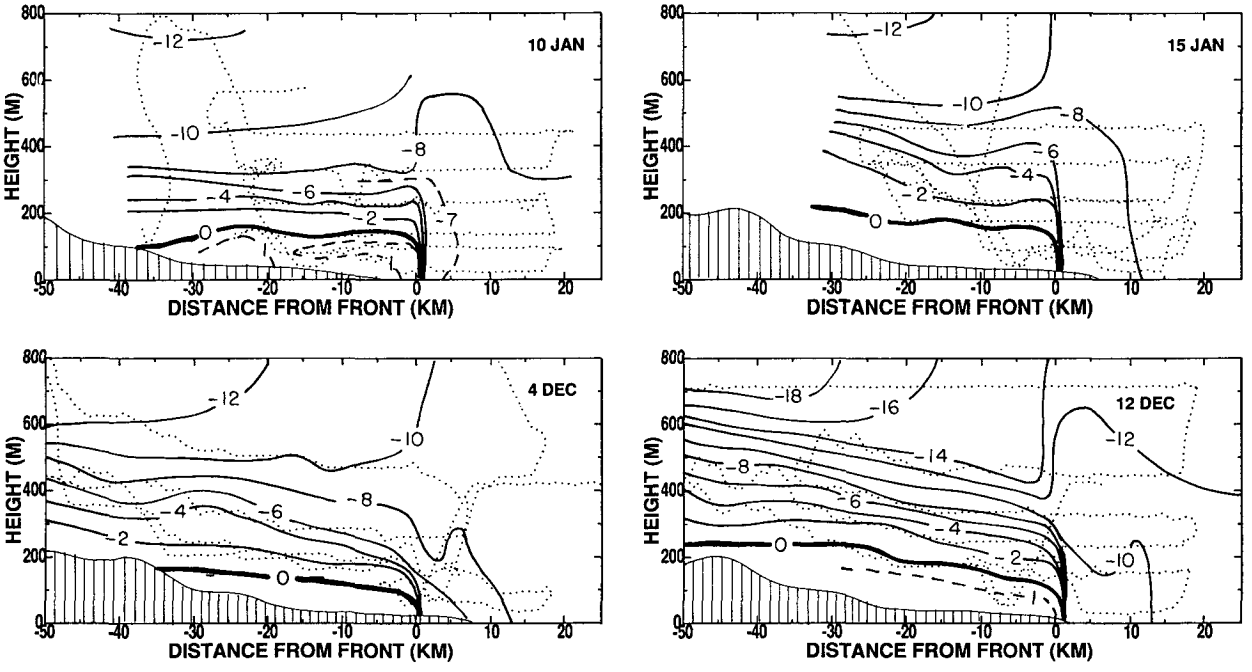

FIG. 3. As in Fig. 2, except of front-normal, front-relative horizontal wind speed (m s^{-1}) subjectively analyzed. Positive wind speed indicates flow toward the right (toward the southeast).

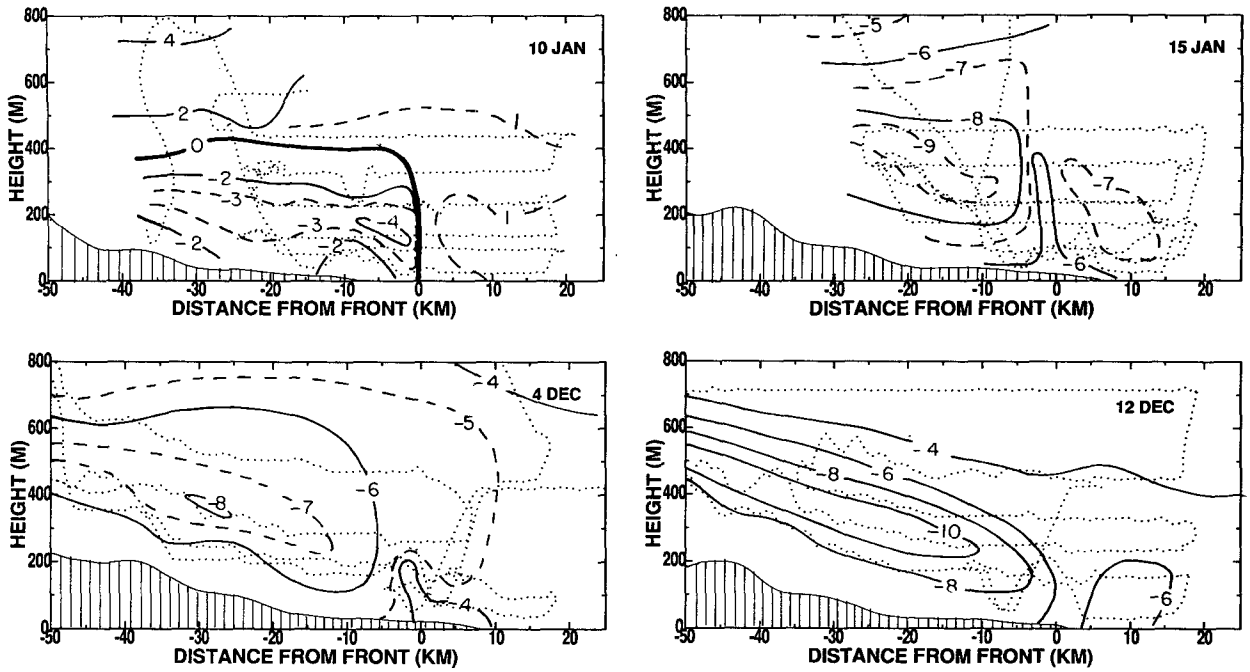

FIG. 4. As in Fig. 2, except of front-parallel horizontal wind speed (m s^{-1}) subjectively analyzed. Positive wind speed indicates flow into the page (toward the northeast.)

determine the equilibrium shape and slope of the frontal inversion and the magnitude of the northeasterly jet beneath it.

Although Bell and Bosart worked with conventional rawinsonde data from the Carolinas, their analysis makes several predictions of smaller-scale structure that are verified qualitatively with the aircraft data. In particular, the maximum northeasterly winds are located at the base of the frontal inversion and are associated with the most steeply sloping portions of the inversion and the deepest thicknesses of cold air. These characteristics are found in each of the four coastal fronts. The 10 Jan front also possesses a front-parallel wind maximum just behind the front and over water, where the surface drag would be smallest.

Because of a lack of aircraft and rawinsonde data, the analyses of the cold-air damming inversion cannot be extended back to the mountain barrier. The barrier, the northern Appalachian mountain range, is located 150 to 250 km inland of the coastal fronts at an elevation of 400 to 1200 m above sea level. The inversions, which are 450 to 650 m above sea level at −50 km and show no sign of weakening, must slope upward toward the mountains everywhere to balance the Coriolis force. Therefore, it is likely that the inversion is higher than the barrier in many places, so that the cold air is not completely trapped upwind of the mountains.

c. *Comparison with other atmospheric fronts*

Coastal fronts tend to possess very narrow surface frontal zones compared to most atmospheric fronts. The sharpness of the frontal zones is emphasized in Fig. 5, which shows potential temperature and front-normal wind at 1-second intervals from the lowest aircraft pass through the 12 Dec front. The 12 Dec front had the largest temperature contrast of the four fronts studied. The aircraft passed through the front at a height of about 140 m above ground level.

The measuring frequency of the aircraft proved inadequate to resolve the narrow frontal zone. The aircraft, flying from right to left relative to the figure, encountered nearly constant winds and temperatures until reaching the frontal zone at 0 km. At the leading edge of the frontal zone, successive 1-second front-normal wind speed observations, spaced 85 m apart, were −10.1 m s^{-1}, −5.6 m s^{-1}, and −2.6 m s^{-1}. This intense part of the frontal zone was at most 170 m wide, implying a horizontal convergence at the frontal zone of at least 4.5×10^{-2} sec^{-1}. The largest observed 2-second potential temperature change, 3.8°C, was colocated with the narrow convergence zone. Thus, the magnitude of the confluent frontogenesis term, $-(\partial u/\partial x)(\partial\theta/\partial x)$, was at least 9.9×10^{-4} K m^{-1} s^{-1}, slightly larger than was obtained from tower measurements of a Colorado cold front (Shapiro 1984), and an order of magnitude larger than aircraft observations of a cold front over the Pacific (Bond and Fleagle 1985).

The frontal inversion/shear layer remains 100 to 300 m thick from behind the head to 50 km behind the front—the extent of aircraft observations—and possibly as far back as the mountain barrier 150 to 250

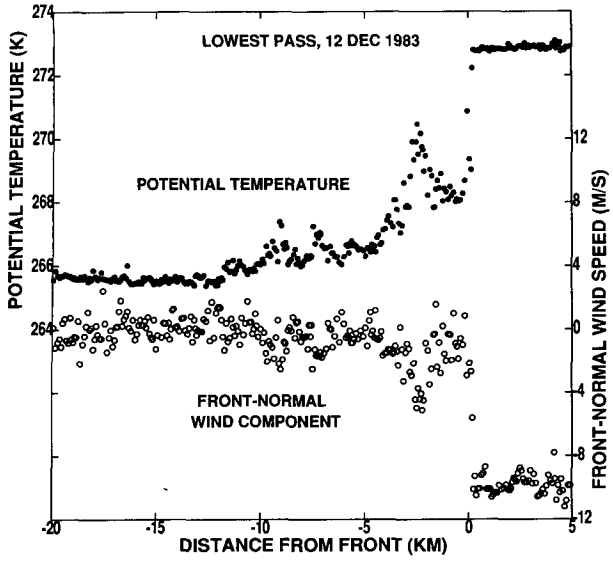

FIG. 5. Graph of potential temperature (upper plot, solid circles, scale to left) and front-normal, front-relative wind speed (lower plot, open circles, scale to right) from lowest aircraft pass through the 12 Dec 1983 coastal front. The data are unsmoothed 1-second observations, taken at 140 m to 170 m above sea level through the frontal zone.

km behind the front. Such a large horizontal extent of the frontal inversion has also been observed in some cold fronts. Ball (1960) analyzed a cold front whose shear layer increased in thickness only 25% between 20 km and 170 km behind the front. Brundidge (1965) presented an unusually shallow cold front (his Case 9) whose inversion, only 150–200 m thick, persisted over 100 km behind the front. Ballentine's (1980) coastal front simulation also shows the inversion remaining narrow, 100 km behind the surface front.

Below the inversion, all four front-normal wind cross sections (Fig. 3) show a 100 m to 200 m deep region of flow toward the front. This structure, while common in the laboratory, is not observed in all atmospheric fronts. The cold fronts analyzed by Browning and Harrold (1970) and Carbone (1982) had their strongest cold-air inflow aloft, near the base of the frontal inversion. Sea breeze fronts often develop into closed rotors, with the inflow limited horizontally to the lower portion of the rotor (Clarke 1961; Simpson et al. 1977). Both of these structures have been reproduced by numerical models, and appear to be caused respectively by surface drag (Mitchell and Hovermale 1977) and the density current outrunning its source of cold air (Garratt and Physick 1986). In coastal fronts, the lack of frontal motion relative to the ground and a continuous supply of cold air from the north due to cold-air damming allow a deep inflow to develop along the ground.

d. Vertical motion and precipitation enhancement

To make apparent the large-scale vertical motion patterns associated with the coastal fronts, a streamfunction analysis was performed using data from the 12 Dec case. The method used to construct the streamfunction is described in appendix B. The analysis is shown in Fig. 6. Because of the data limitations, the analyzed streamline structure above 1000 m is only intended to be suggestive of the actual structure.

The large-scale vertical structure depicted in Fig. 6 is typical of the four coastal fronts studied. The marine boundary layer air ahead of the coastal fronts possessed nearly neutral stratification. In all but the 10 Jan case, this marine air was being heated from below by the Gulf of Maine, which was 2° to 6°C warmer than the overlying air. At heights of 1 to 2 km, the marine layers were capped by warm frontal inversions, as is typical of the environments of coastal fronts of this type (McCarthy 1977).

The vertical potential temperature structure 50 km inland of the 12 Dec front, deduced from aircraft data, is also depicted in Fig. 6. The coastal front inversion is located between 400 and 600 m above sea level. The warm front inversion extends from 1300 m to 1700 m. Between the two inversions is the marine layer, which has been advected inland from ahead of the coastal front.

The streamfunction analysis shows that the marine air layer, as it passes over the head of the coastal front, becomes constricted between the coastal front inversion and the warm front inversion. Under the assumption of two-dimensionality, mass continuity demands that the velocity must increase as the depth of the layer decreases. This acceleration may be seen as a sudden jump in velocity over the front above the 500 m level in Fig. 3d and an increased vertical gradient of the streamfunction above the coastal front in Fig. 6. This sort of acceleration over the leading edges of fronts is actually quite common, and has been observed by Browning and Harrold (1970) and Hobbs and Persson (1982), among others. Farther behind the surface coastal front position, the marine air accelerates much more gradually as it passes over the sloping coastal front inversion.

At and above each front, a primary updraft 400 m to 1200 m wide, with vertical velocities of up to 2.5 m s^{-1}, was observed directly by the aircraft. The coastal front updraft resembles the frontal updrafts observed by Shapiro et al. (1985), Young and Johnson (1984), and Wakimoto (1982), with maximum upward motion in the warm air at the leading edge of the front, tilting back towards the cold air with height. The updraft reaches a maximum near the top of the coastal front inversion layer and decreases above, as has been observed in cold fronts (Browning and Harrold 1970; Bond and Fleagle 1985). As can be seen in Fig. 6, the updraft velocity approaches zero near the base of the overlying warm frontal inversion. The updraft is weaker than in other atmospheric fronts because of the relative shallowness of the coastal fronts and the relatively weak front-relative warm air wind speeds.

The mechanical lifting of warm air by the coastal

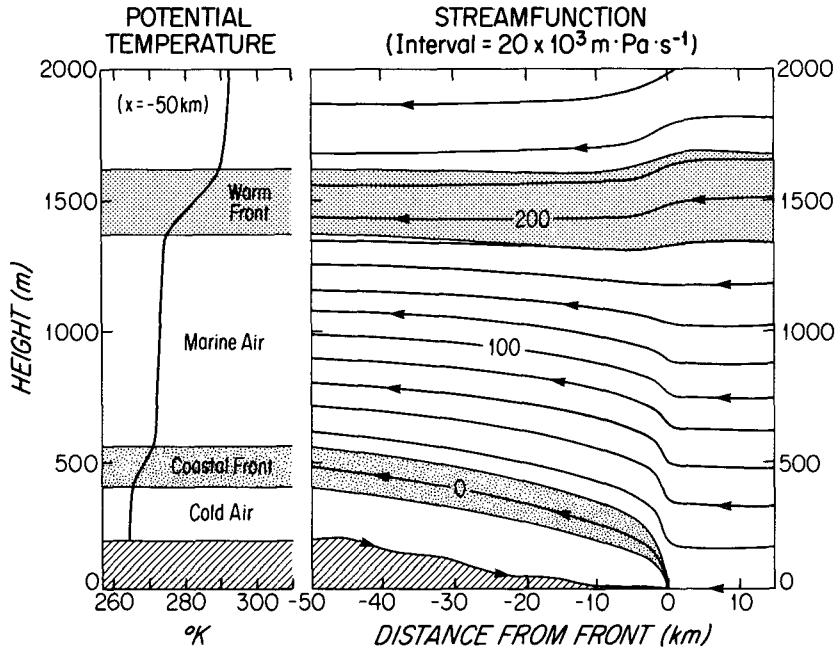

FIG. 6. Analysis of vertical structure of temperature and wind associated with 12 Dec coastal front event. The potential temperature 50 km inland of the coastal front is plotted on the left. This temperature structure was pieced together from aircraft soundings 50 km inland and 15 km offshore of the coastal front. On the right is the streamfunction Ψ normal to the plane of the coastal front, where Ψ is defined such that $\partial\Psi/\partial p = u$ and $\partial\Psi/\partial x = -\omega$. See appendix B for details of the streamfunction analysis methods. The spatial distribution of the coastal front inversion was determined from direct aircraft measurements. The distribution of the warm front inversion is from extrapolation, using the streamfunction analysis, of aircraft measurements 15 km offshore of the coastal front.

front and cold pool inversion was suggested by Marks and Austin (1979) as the mechanism for observed enhancement of precipitation within a 50 km wide band along coastal fronts. Because of the nature of cold-air damming, the vertical displacement caused by the coastal fronts and associated cold pools is similar to the orographic lifting that would take place farther inland in the absence of cold air damming. Consequently, the coastal front effectively shifts much of the orographic enhancement of precipitation from the mountain slopes to the coastal plain during onshore flow.

Figure 6 shows that the mechanical lifting at the front is confined to the marine layer beneath the warm frontal inversion. At and above the inversion, the vertical motion distribution should be similar to solutions to the time-dependent 1½-layer problem of subcritical flow over a two-dimensional obstacle, with the warm front inversion approximated by a discontinuous jump in density. For Froude numbers appropriate to typical coastal front situations, theoretical analyses and numerical simulations by Baines and Leonard (1989) predict that as the marine layer air approaches the coastal front, it should become deeper and decelerate, producing upward motion with a maximum at the warm frontal inversion. The upward motion should have a horizontal scale of 100 km to 300 km, with a total vertical displacement at the level of the warm front of 100 m to 200 m. Thus, while a narrow region of strong vertical motion is located at low levels above the coastal front, a broader, deeper region of weak upward motion should be present ahead of the coastal front. Incidentally, the deceleration and upward motion would be associated with a hydrostatic pressure gradient directed toward the front, again with a scale of 100 km to 300 km. This may explain the unexpected observation by Bosart et al. (1972) of cross-isobar flow toward higher pressures in the warm air ahead of a coastal front.

During passes through the 15 Jan front, very light snow was noted by the flight observer (P. Neilley) on the cold side of the front. The snow originated from a stratocumulus cloud deck within the marine layer, between 1.1 km and 1.8 km above ground level. By estimating fall speeds from particle diameters (Locatelli and Hobbs 1974), particle trajectories were calculated back from the observing points to the clouds. It was found (see Fig. 7) that the peak precipitation rates were associated with trajectories that originated in the clouds directly over the front. The MIT radar observed a narrow 10 dbZ echo along the front during this period, and where precipitation was more widespread farther south, a 5 dbZ reflectivity enhancement coincided with the coastal front position. It must be emphasized that the aircraft-observed precipitation was very light, av-

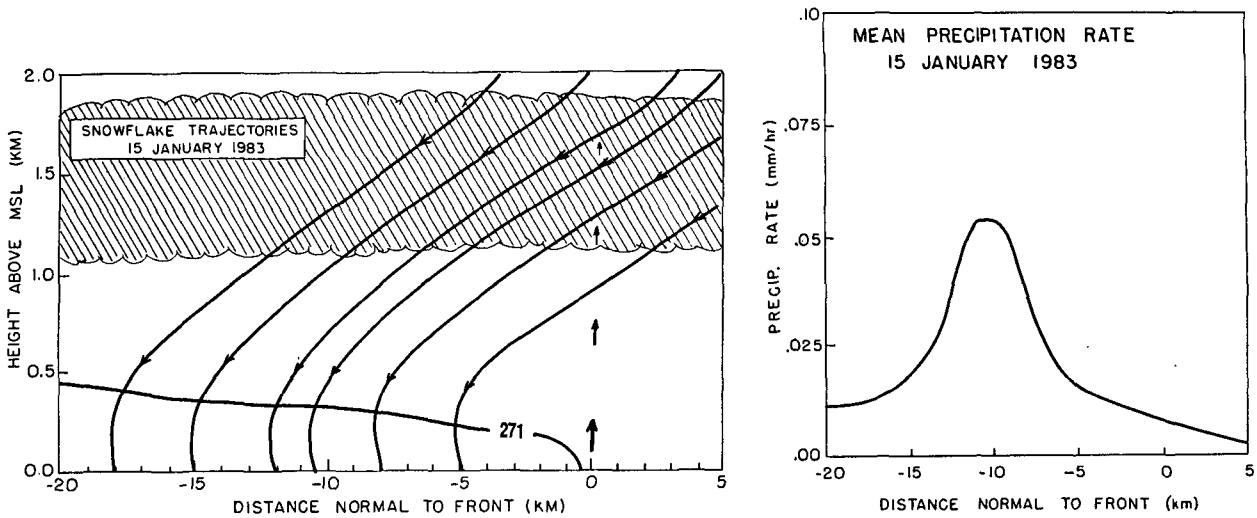

FIG. 7. Schematic diagram of 15 Jan coastal front and overlying clouds, showing calculated snowflake trajectories, presumed location of frontal updraft, and observed precipitation rate. The position of the coastal front is indicated by the 271 K potential temperature isotherm. The precipitation rate was computed with data from a PMS probe averaged over all passes through the 15 Jan coastal front and plotted as a function of distance normal to the front.

eraging 0.06 mm h^{-1} over the period of observation. The aircraft was unavailable during heavier precipitation events because of visibility and icing problems, so no direct evidence was obtained of precipitation enhancement due to the mesoscale vertical motion expected ahead of the coastal front near the level of the warm front inversion.

4. Density current characteristics

a. Observed density current structures

Many types of atmospheric fronts have been found to have the characteristics of density (gravity) currents (Simpson 1987; Simpson 1982). Density current structure has been observed in sea breeze fronts (Simpson 1969; Simpson et al. 1977), thunderstorm gust fronts and haboobs (Goff 1976; Charba 1974; Lawson 1971), and cold fronts (see Smith and Reeder 1988 for a critical review). Density current characteristics visible in Figs. 2 and 3 include the following:

1) Near the ground, the cold and warm air are two separate, nearly homogeneous fluids, with most of the horizontal density (potential temperature) gradient confined to a frontal zone much less than 500 m wide.

2) Beneath the inversion, there is a "feeder flow" of cold air from the cold pool toward the coastal front.

3) The frontal zone rises sharply from the ground to a height of 200 m to 300 m. Examination of 1-second aircraft data (for example, see Fig. 5) indicates that immediately behind this frontal zone, or "head," is a region of turbulence where mixing of the cold and warm air is apparently taking place.

4) The frontal inversion is nearly level behind the head, with typical slopes of 1:50 to 1:200.

Figure 8 shows the potential temperature and airflow structure of the head of the 12 Dec coastal front, with an aspect ratio of 4:1. The arrows depict smoothed 3-minute air parcel displacements and have been analyzed from 8-second averages of aircraft-observed horizontal and vertical velocity. The subjective potential temperature analysis is based on unsmoothed 1-second data. Because of the time difference between successive passes, the small-scale temperature structure analyzed between 0 km and −5 km should not be interpreted as an instantaneous depiction of actual structure, but rather as an indication of the magnitudes and scales of temperature variations that were observed in that region.

After allowing for the 4:1 aspect ratio, good agreement is found between this coastal front and images of laboratory density currents that are nearly stationary relative to the bottom of the tank (for example, see Fig. 2a of Simpson and Britter 1980). The warm air is seen to flow up over the cold air and become partially entrained in the inversion, while the cold air below the inversion flows toward the head, rises, and is entrained within the inversion. Beyond the mixing region at 0 km to −5 km, the inversion/shear zone is nearly flat and much less chaotic. The coastal front is also similar in form to the free-slip numerical simulations of density currents by Droegemeier and Wilhelmson (1987).

The remaining three fronts were found to have similar structure (not shown), but the 4 Dec front possessed a relatively shallow frontal slope of 1:12 ahead of the mixing region (see Figs. 2–3 and appendix A). This front in part resembles a type of density current known as a density or saline wedge which, as discussed

by Britter and Simpson (1978), is obtained in the laboratory when a density current is brought to rest or retreats over a fixed lower boundary. Although all four fronts were moving into the warm air, the 4 Dec front was the only front that was retreating with respect to the ground. It was also farthest from the coast, so that the frictional retardation of the warm air, which leads to density wedge structures (Jirka and Arita 1987), would have been greatest.

b. *Applicability of density current theory to coastal front motion*

Two nondimensional parameters of a steady-state, inviscid density current are the internal Froude number K and the normalized depth h. The Froude number is defined as $U_r/(g'H_c)^{1/2}$, where $U_r = C - U_w$ is the speed of the density current relative to the warm air (with C being the density current speed relative to the ground and U_w being the speed of the warm air relative to the ground); $g' = g\Delta\theta/\theta_o$ is the reduced gravity (with $\Delta\theta$ being the virtual potential temperature difference across the front and θ_o being the mean virtual potential temperature); and H_c is the depth of the density current. The normalized depth h is H_c/H_w, the ratio of the depth of the current to the depth of the warm air ahead of the current. Throughout this discussion we will use the subscripts c and w to refer to the cold air within the density current and the warm air ahead of the density current, respectively.

Benjamin (1968, hereafter B) investigated the theory of a density current with no surface drag and no mixing between the warm and cold air. B found that for a steady state current, only a single value of K was possible for a given h. Specifically,

$$U_r/(g'H_c)^{1/2} = K(h) \tag{1a}$$

with

$$K(h) = \left(\frac{(1-h)(2-h)}{(1+h)}\right)^{1/2}. \tag{1b}$$

The magnitude of K increases monotonically from $1/\sqrt{2}$ for a deep density current ($h = 0.5$) to $\sqrt{2}$ in the limit of a shallow density current ($h = 0$). To use this result to predict the speed of a density current, Eq. (1a) may be rearranged to give

$$U_r = C - U_w = K(g'H_c)^{1/2}. \tag{2}$$

Britter and Simpson (1978, hereafter BS) considered the effect of mixing between the cold and warm air, and found that the amount of mixing between the two fluids affected the value of K for a given h. The amount of mixing, or equivalently the amount of inflow of cold air toward the density current, must be specified observationally or experimentally. A specific K–h relation was obtained by BS by assuming a Richardson number through the mixing layer consistent with laboratory experiments of Kelvin–Helmholtz instability.

A principal cause of differences between inviscid theory and observations of density currents is the effect of the lower boundary in slowing down the cold air through surface drag. In a later paper, Simpson and Britter (1980) surveyed observations of density current propagation for a variety of nondimensional depths h. By plotting C as a function of U_w, Simpson and Britter found that the effect of friction on (2) could be parameterized as

$$C = K(g'H_c)^{1/2} + bU_w \tag{3}$$

where K is reduced from its inviscid value and b was found by linear regression to be roughly 0.7. Simpson and Britter also conducted laboratory experiments and developed a semiempirical theory incorporating surface

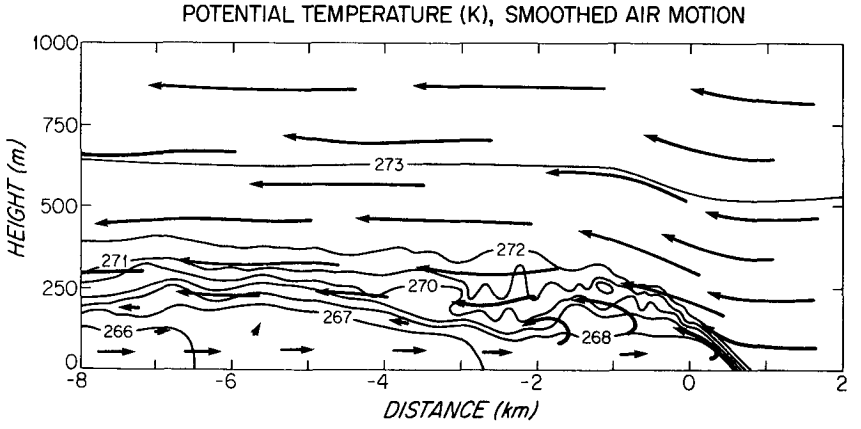

FIG. 8. Cross section normal to 12 Dec 1983 coastal front. Potential temperature has been subjectively analyzed from 1-second observations. Arrows represent parcel trajectories in the plane of the cross section, with the length of an arrow representing the motion of an air parcel over a three-minute period. Small-scale motions associated with turbulent mixing along the frontal interface are not depicted. The aspect ratio is 4:1.

drag, valid in the neighborhood of $U_w = 0$, which confirmed this result. Equation (3) has become a standard means of comparing observed frontal motion to density current theory (Smith and Reeder 1988 and refs.).

Coastal fronts, however, lie outside the parameter range of the atmospheric density currents surveyed by Simpson and Britter, as well as lying outside the range of validity of their theory incorporating surface drag. For coastal fronts, U_w is negative and much larger than $|C|$. Inspection of the theory of Simpson and Britter shows that as U_w becomes negative, the parameter b approaches 1, and (3) reduces to (2). This makes intuitive sense, for as the velocity of the opposing warm air increases and the density current slows, friction within the cold air should have a lesser effect on the dynamics of the density current.

Thus coastal fronts offer an excellent opportunity to compare the simple, inviscid density current theory of B and the modified theory of BS to actual atmospheric fronts. Because the fronts are quasi-stationary, with flow toward the front within the cold air of only 1–2 m s^{-1}, the effect of friction on the cold air is minimized. Also, the warm air ahead of coastal fronts is very weakly stratified, so the complication of density current propagation into a stably stratified environment is avoided.

Coriolis effects are not expected to be directly important to the density current dynamics because, even though a coastal front will persist for 18 hours or more, parcel residence times within the head of a coastal front tend to be 10 to 30 minutes, much less than the local inertial period. Inspection of Fig. 4 shows no systematic along-front velocity maximum in the cold air within 2 km of the leading edge of the fronts, where the steeply sloping frontal discontinuity would imply a substantial wind shear if thermal wind balance were locally valid. As discussed earlier, the Coriolis force is important to the dynamics of cold-air damming, so its influence may be felt in two ways: through modulation of the depth of the coastal front, and through variations in the flow of cold air toward the front. The implications of an interaction between cold-air damming dynamics and density current dynamics will be addressed in section 6.

c. *Comparison of theoretical and observed coastal front speeds*

Direct comparison of density current velocities predicted by B and BS is complicated by different choices of the definition of H_c made in the two papers. For application of two-fluid theory to atmospheric flows, the appropriate choice for H_c (B, p. 242) is the densi-

TABLE 1. Comparison of coastal fronts with theoretical density current velocities.

(B) = Benjamin 1968 (BS) = Britter and Simpson 1978

Parameters				Coastal front cases			
Description	Source	Symbol	Units	10 Jan	15 Jan	4 Dec	12 Dec
Depth of warm and cold air							
Depth of warm air	observed	H_w	m	1100 ± 100	1700 ± 300	1100 ± 200	1200 ± 100
Densimetric depth of cold air	observed	$H_c^{(B)}$	m	220 ± 30	350 ± 40	225 ± 30	260 ± 20
Height of base of inversion	observed	$H_c^{(BS)}$	m	140 ± 20	200 ± 20	170 ± 30	180 ± 20
Nondimensional height, after B	$H_c^{(B)}/H_w$	$h^{(B)}$		0.20 ± 0.05	0.21 ± 0.06	0.21 ± 0.07	0.22 ± 0.04
Nondimensional height, after BS	$H_c^{(BS)}/H_w$	$h^{(BS)}$		0.13 ± 0.03	0.12 ± 0.02	0.16 ± 0.06	0.15 ± 0.03
Thermal parameters							
Virtual potential temperature difference	observed	$\theta_w - \theta_c$	K	5.3 ± 0.2	3.4 ± 0.3	3.3 ± 0.6	6.6 ± 0.5
Reduced gravity	$g\Delta\theta/\theta_o$	g'	m s^{-2}	0.19 ± 0.01	0.12 ± 0.01	0.12 ± 0.02	0.24 ± 0.02
Internal velocity, after B	$(g'H_c^{(B)})^{1/2}$		m s^{-1}	6.5 ± 0.6	6.6 ± 0.7	5.2 ± 0.8	7.9 ± 0.6
Internal velocity, after BS	$(g'H_c^{(BS)})^{1/2}$		m s^{-1}	5.2 ± 0.5	5.0 ± 0.5	4.5 ± 0.8	6.6 ± 0.6
Theoretical predictions							
Froude number, after B	Equation 1b	$K^{(B)}$		1.10 ± 0.07	1.09 ± 0.09	1.09 ± 0.09	1.07 ± 0.03
Froude number, after BS	Fig. 6b of BS (with $R_L = 0.35$)	$K^{(BS)}$		1.32 ± 0.12	1.35 ± 0.07	1.22 ± 0.16	1.25 ± 0.08
Relative speed of front, after B	$K^{(B)}(g'H_c^{(B)})^{1/2}$	$U_r^{(B)}$	m s^{-1}	7.1 ± 0.6	7.1 ± 0.8	5.7 ± 0.9	8.5 ± 0.7
Relative speed of front, after BS	$K^{(BS)}(g'H_c^{(BS)})^{1/2}$	$U_r^{(BS)}$	m s^{-1}	6.8 ± 0.6	6.7 ± 0.7	5.5 ± 1.0	8.2 ± 0.7
Observed coastal front velocities							
Speed of front with respect to ground	observed	C	m s^{-1}	1.35 ± 0.2	0.8 ± 0.1	−0.6 ± 0.1	0.2 ± 0.15
Speed of warm air w.r.t. ground	observed	U_w	m s^{-1}	−5.4 ± 0.4	−6.2 ± 0.5	−6.4 ± 0.8	−9.4 ± 0.6
Relative speed of front, observed	$C - U_w$	U_r	m s^{-1}	6.75 ± 0.45	7.0 ± 0.5	5.8 ± 0.8	9.6 ± 0.6

metric height. The densimetric height may be defined as the depth a cold layer would have if the surface potential temperature and hydrostatic pressure were held fixed and the vertical potential temperature gradient were confined to an infinitesimally thin layer. BS, on the other hand, defined H_c as the depth of the unmixed cold air. For the case of linear potential temperature gradient confined to an inversion layer, the densimetric height $H_c^{(B)}$ (H_c as defined by B) is the height of the middle of the inversion, while $H_c^{(BS)}$ (H_c as defined by BS) is the height of the base of the inversion.

The density current characteristics of the four coastal front cases are given in Table 1 and compared to theoretical predictions of the speed of a density current relative to the warm air. Lacking complete vertical profiles of wind and temperature on both sides of the coastal fronts, we have used 1 km averages from aircraft passes located at 10 km and 5 km behind the front and at +2 km, and +5 km in the warm air ahead of the front to estimate the characteristics of the warm and cold air. The proper choice for U_w was not obvious because of the presence of wind shear in all but the 10 Jan front, likely caused by surface friction as the air passed over land. We have chosen U_w to be the mean warm air velocity averaged over a depth equal to $H_c^{(B)}$. The depth of the warm air (H_w) was taken to be the distance from the ground to the base of the warm frontal inversion capping the neutrally stratified layer, and was determined from aircraft penetrations of the inversion (when available) and from rawinsonde observations. All error estimates are based on differences among averaging locations and successive passes. In the case of H_w, they also include estimates of errors due to poor spatial and temporal sampling of the warm frontal inversion height by rawinsondes.

The observed speeds are found to be quite close to those predicted by theory. The only notable discrepancy is found with the 12 Dec front, for which the uncertainty ranges of the observed and theoretical frontal velocities barely overlap. Observations of the remaining three fronts match inviscid steady-state density current velocities to within 0.35 m s^{-1}, well within the accuracy of the observations. The inclusion of mixing in density current theory causes the theoretical predictions of BS to be smaller than those of B by a minor amount, 0.2–0.4 m s^{-1}, which does not improve the already good agreement between B and observed speeds. Atmospheric features neglected by both theories, such as friction within the cold air and wind shear within the warm air, were apparently either insignificant or tended to cancel.

5. Instability and mixing along the frontal interface

Behind the head of density currents is a region of rapid turbulent mixing. This mixing has been found to take the form of Kelvin–Helmholtz (KH) billows in the laboratory (Britter and Simpson 1978) and in sufficiently detailed numerical simulations (Droegemeier and Wilhelmson 1987). Tower observations of cold fronts (Young and Johnson 1984; Shapiro et al. 1985) have also found turbulent mixing with the inversions immediately behind the surface fronts.

As seen in Fig. 8, a similar region of turbulence is present just behind coastal fronts. An example of the rapid variations of wind and temperature observed within the frontal inversion behind the head of the coastal front is found in Fig. 5. The potential temperature and wind between 0 km and −10 km vary on length scales ranging from <100 m to 2 km. Second-to-second wind speed variations of 2 m s^{-1} are common. The potential temperature and front-normal wind tend to be anticorrelated, as would be expected for parcels originating on opposite sides of the front.

To determine whether the vertical structure of the coastal front inversions had been influenced by KH instability just behind the front, bulk Richardson numbers were computed by averaging aircraft data horizontally over 3–4 km distances between −3 km and −32 km and computing vertical finite differences using the formula

$$\mathrm{Ri} = g\theta^{-1}\Delta\theta(\Delta U)^{-2}\Delta z \qquad (4)$$

where ΔU is the magnitude of the vector wind shear between levels and other symbols have their usual meaning. The horizontal averaging was over distances larger than any observed wavelike motions. Across the frontal inversions, individual estimates of Ri varied between 0.19 and 0.52, with a mean of 0.31. The few vertical penetrations of the coastal front inversion by aircraft indicated that the wind and potential temperature tended to vary linearly with height. Both of these results are consistent with laboratory studies of inversions after KH mixing (Thorpe 1973). Below the inversion, wind shear was typically still present while the stratification was nearly neutral, so that Ri tended to be less than 0.25 in that region. Above the inversion, where the second-to-second variations in wind speed observed by aircraft were weakest, Ri was generally between 0.5 and 1.0.

At the leading edge of the front, KH instability would require that the local Ri be less than 0.25 (Miles and Howard 1964). An estimate of this Ri may be made using the pass shown in Fig. 5, ignoring the decrease in effective stability caused by the slope of the frontal interface. If the interface is nearly horizontal, the initial Richardson number of the front may be approximated as

$$\mathrm{Ri} = g\theta^{-1}\Delta\theta(\Delta U)^{-2}\Delta x \sin\beta \qquad (5)$$

where β is the angle of the frontal interface above horizontal and Δx is the observed horizontal width of the frontal zone (see Fig. 9). Using previously quoted values of $\Delta\theta = 3.8$°C and $\Delta u = 7.5$ m s^{-1} (variations in v and w across the front were less than 1 m s^{-1}), (5) becomes

$$\mathrm{Ri} = 2.5 \times 10^{-3}\Delta x \sin\beta. \qquad (6)$$

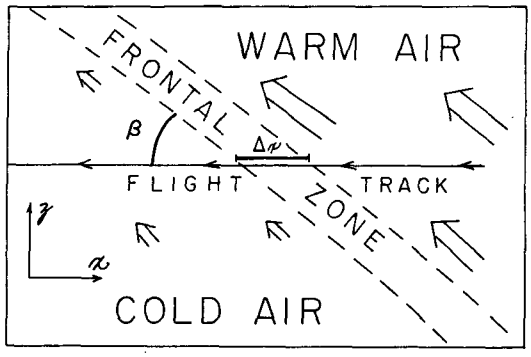

FIG. 9. Schematic drawing of aircraft pass through the frontal zone, showing definitions of β and Δx used in estimate of Richardson number across the frontal zone.

The actual size of Δx is not known, but an upper bound on the width of the frontal zone is 170 m, the distance covered by the aircraft in the two seconds between observations on the warm and cold sides of the front. Three estimates of β are available. Two, as described in appendix A, are from a least-squares fit of frontal locations. On 12 Dec, there were three passes through the front between 140 m and 245 m. Estimates of the slope of the front based on gradients of wind and temperature are -0.15 and -0.19. Because of the likely curvature of the frontal interface, the actual magnitude of the frontal slope at 140 m is probably larger. A third measure of the slope of the front may be obtained by computing the instantaneous slope (w/u) of the air in the center of the frontal zone at 140 m. At that point, $u \sim -5$ m s^{-1} and $w \sim 1.2$ m s^{-1}, which yields a slope of -0.24, consistent with the expected bias in the other two estimates. Using $\beta = \tan^{-1}(-0.24 \pm 0.09)$ yields

$$\mathrm{Ri} \leq 0.10 \pm 0.04, \qquad (7)$$

which is well below the necessary condition for KH instability.

6. Discussion

We have presented aircraft observations of the vertical structure of four New England coastal fronts. Based on the similar structure exhibited by all four fronts, we infer that the observations are characteristic of all mature type A and type B coastal fronts. No aircraft observations were available of type C coastal fronts, which are produced by upstream blocking by orography rather than a land–sea thermal contrast (Nielsen 1989), but our observations are consistent with the vertical structure calculated by Garner's (1986) numerical model of frontogenesis by upstream blocking. Differences in frontal behavior may be expected, due to the stably stratified warm air in the type C cases. This stratification could affect frontal velocities by inducing borelike disturbances in the warm air (Smith and Reeder 1988).

By mature coastal fronts we mean fronts accompanied by cold-air damming, in which the coastal front inversion extends back to the inland mountains as the top of a pool of cold air. The time scale for maturation should be comparable to the time required for air originally within the marine boundary layer to advect eastward to the mountains. In New England, with a distance of 200 km and mean winds of 5–10 m s^{-1}, this advective time scale is 6–12 hours. All aircraft observations in this study were made at least 12 hours after coastal front formation.

The coastal fronts were shown to possess the characteristics of a slow-moving atmospheric density current. The observed frontal velocities are in close agreement with the inviscid density current theoretical predictions of Benjamin (1968), as well as the theory of Britter and Simpson (1978) incorporating mixing.

At the leading edge of the cold air, the frontal zone slopes back from the ground to a height of 300–450 m over a horizontal distance of 0.5 to 2.5 km. The marine air reaching the head is forced upward by the cold air, reaching vertical velocities of up to 2–3 m s^{-1} in a band 1–2 km wide while accelerating toward the mountains. The cold air flows toward the front at low levels, is forced upward at the head, and mixes turbulently with the warm air in the frontal inversion. Ahead of a coastal front, a 100–300 km wide area of weak ascent is anticipated, with maximum vertical displacement at the level of the inversion capping the marine layer.

The coastal front inversion slopes gradually upward toward the mountains, with a pool of cold air beneath it. The wind and temperature structure within the cold pool resembles the case of Appalachian cold-air damming studied by Bell and Bosart (1988), with a northeasterly jet present in the cold air at the base of the inversion. The northeasterly jet supplies a continual influx of cold air which reinforces the damming and helps compensate for the loss of cold air by leakage over the mountain barrier or by mixing into the warm air through the inversion.

Further study is necessary to determine how the cold-air damming inversion forms. It seems likely that the inversion forms initially at the coastal front and propagates westward as the onshore flow intensifies, but it is possible that cold-air damming may occur independently. We note that cold-air damming frequently occurs without coastal frontogenesis, especially when sea surface temperatures are colder than air temperatures. Conversely, certain coastal fronts are so short-lived that damming never develops. In the Carolinas, coastal fronts form along the Gulf Stream (Riordan et al. 1985; SethuRaman and Riordan 1988), far from the initial influence of cold-air damming. They frequently move inland discontinuously (George 1960), possibly reforming along the edge of the pool of cold air.

In New England, with the mountains relatively close to the coastal temperature gradient, coastal fronts and cold-air damming tend to exist as a coupled system. Although they have been described here in terms of

entirely separate dynamical processes, there is no difficulty in postulating a mutual interaction in which the coastal front forms the leading edge of the cold pool. The equilibrium shape of the cold pool is determined by the temperature difference and the large-scale pressure gradient. Similarly, the height of a stationary density current is determined by the temperature difference and the structure of the warm air flow. Where the equilibrium depth of the cold pool is equal to the densimetric height of a stationary density current, the coastal front would tend to come to rest.

By this scenario, if the surface heating discontinuity where the coastal front forms is east of the location at which cold-air damming would support a stationary density current, the dynamics controlling the cold-air damming would prevent cold air from flowing toward the front to replenish the cold air lost to mixing at the front. The depth of the coastal front would then decrease, causing the front to retreat westward until the depth of the cold air was sufficient to allow the front to become stationary. In most atmospheric density currents, such as gust fronts, one thinks of the speed of the density current as being determined by the depth and temperature of the cold air. In the case of a steady coastal front/cold-air damming system, however, given a temperature contrast and an ambient onshore wind, the speed of the coastal front is zero and the depth of the cold air determines the coastal front's location.

The predictive power of the above conceptual model could be tested by the use of a three-dimensional steady-state mesoscale model capable of accurately simulating the airflow associated with a cold-air damming episode. After determining the structure of the equilibrium height of the cold dome as a function of the temperature difference and the ambient pressure gradient, surface observations of coastal front location could be compared to that predicted by the density current equation (2), substituting for H_c the model-determined equilibrium cold dome height.

Short-range forecasts of coastal front motion could also make use of the concept of the coastal front as a density current. From (2), changes in the warm air wind speed U_w should lead directly to changes in the speed of the coastal front. This would be an easily applied prognostic tool, since the change in frontal speed would be independent of other theoretical or physical parameters such as K or H_c.

Acknowledgments. We wish to acknowledge the contributions of all those who participated in NEWSEX, especially Principal Investigator Dr. Richard Passarelli and the NCAR Research Aviation Facility personnel. Discussions with J. Klemp and R. Rotunno clarified several aspects of density current theory. The figures were drafted by Mike Rocha and Isabelle Kole. This work was supported by National Science Foundation Grants ATM-8209375 and ATM-8607132, and by the generosity of the Henry G. Houghton Fund.

APPENDIX A

Determination of Frontal Velocities

The determination of frontal velocity is an important element of any frontal case study. In case studies using Doppler radar, frontal velocity must be known to deduce the front-relative flow structure. Case studies using tower observations or sequential soundings also require frontal velocity to determine the proper space–time conversion and horizontal scales. With aircraft cross sections, knowledge of even the vertical structure of the front depends critically on applying the proper space–time correction.

For example, the aircraft observations of the 10 Jan front consist mostly of eight passes at increasing altitudes. The passes were roughly evenly spaced in time and altitude. Consequently, determination of the slope of the front requires knowledge of the speed of the front, and vice versa. If the lowest and highest passes are separated by 1.5 hours, an error of 0.5 m s^{-1} in frontal velocity will produce an error of 2.7 km in the relative positioning of the two passes. Independent knowledge of the speed of the front, say from a series of frontal passes at surface stations, it is not available because of the front's low speed. Bond and Fleagle (1985), who had only three aircraft passes and no surface data, were forced to position the aircraft passes by assuming a vertical frontal updraft.

This problem of needing to assume frontal structure may be avoided by making two aircraft passes at a single level, thereby determining the speed of the front independent of frontal shape. For the 15 Jan front, two passes were made at 235 m, and three passes were made at 70 m to 110 m. However, the various sets of passes produced conflicting estimates of frontal velocity, ranging from 0.6 m s^{-1} to 1.1 m s^{-1}. These differences are possibly due to spatial and temporal variations in frontal structure, actual variations in the speed of the front, errors in the position of the aircraft as determined from the inertial navigation system, or errors in determining the horizontal orientation of the front from surface analyses.

Because of these conflicts, we have used data from as many passes as possible to determine frontal velocity. For each pass, the location, time, and elevation were noted of the easternmost gradient of front-normal wind. Then, for various frontal speeds, a time-to-space conversion was applied, the least-squares best-fit line was calculated through the frontal pass data points, and the root-mean-square horizontal deviation of the data points from the best-fit line was evaluated. This process was repeated for frontal locations determined from the easternmost temperature gradient, the peak vertical motion averaged over 200 m, and the peak vertical motion averaged over 1000 m, yielding four sets of best-fit lines and rms deviations. The frontal speed was then chosen to be that speed which minimized the sums of the rms deviations. The results of these calculations are given in Table A1.

TABLE A1. Frontal velocities computed from linear least-squares best fit to location of wind shift (ΔU), temperature break ($\Delta\theta$), 200 m wide maximum updraft location (W^{200}), and 1000 m wide maximum updraft location (W^{1000}). Also given are the slopes of the best-fit lines and the root-mean-square deviation (in km) of the data points from the best-fit lines.

		Number of data points				Frontal slopes				Rms deviations (km)			
Frontal speeds (m s^{-1})		ΔU	$\Delta\theta$	W^{200}	W^{1000}	ΔU	$\Delta\theta$	W^{200}	W^{1000}	ΔU	$\Delta\theta$	W^{200}	W^{1000}
10 Jan	1.35 ± 0.2[1]	7	7	7	8	−.21	−.22	−.18	−.26	.15	.15	.13	.17
15 Jan	0.8 ± 0.1	6	6	7	8	−.18	−.14	−.83	−.33	.11	.12	.12	.13
4 Dec	-0.6 ± 0.15[2]	2	3	5	4	−.09	−.12	−.34	−.63	—	.04	.18	.08
12 Dec	0.2 ± 0.2	3	3	5	5	−.16	−.21	−.30	−.25	.00	.02	.07	.10

[1] From closest match of slopes to 12 Dec front.
[2] From W^{200} and W^{1000} only.

This method of determining frontal velocities does not require that the slopes of the best-fit lines be similar. Indeed, as expected, the slopes calculated from the vertical motion tend to be steeper, because they include the updraft within the warm air above the front.

Because of the 10 Jan flight pattern, the standard deviations for that case were nearly independent of frontal speed. We have estimated frontal speed for that case by matching the four best-fit slopes to those calculated for 12 Dec, a front with similar intensity and an assumed similar structure. Also, because of the lack of sufficient data points, the 4 Dec frontal speed was determined using vertical motions only.

Error ranges for frontal velocities were estimated from the sensitivity of the rms deviations to changes in frontal velocity. The rms deviations are all less than 200 m, giving us high confidence in the resulting frontal shapes.

APPENDIX B

Method of Streamfunction Analysis

The streamfunction analysis shown in Fig. 6 was produced from direct aircraft observations of the wind and potential temperature, as well as dynamical considerations. It is meant to represent air velocities averaged locally over periods of about an hour, and does not include wavelike or turbulent motions with the warm air or in the frontal zone. Because of a lack of observations, we have also not attempted to depict vertically propagating gravity waves which may have been induced in the warm front inversion by coastal front.

Between 200 m and 700 m, aircraft observations were of sufficient vertical density to compute the streamfunction directly from wind observations. The streamfunction was determined by vertical integration of front-normal wind along columns spaced 10 km apart, with greater horizontal resolution in the vicinity of the frontal updraft. Aircraft measurements of vertical velocity over the front were used as a consistency check. Below 200 m above ground level, a wind field was assumed that would place the zero streamfunction contour near the center of the coastal front inversion.

Between 700 m and 2000 m, aircraft data were available at only two levels (1100 m and 1700 m). Incorrect vertical interpolation of such sparse data could lead to errors of 100 m to 200 m in the height of streamlines, changing the sign of the inferred vertical motion. Vertical profiles of wind and temperature were only available between 1100 m and 1700 m at +20 km and above 1700 m at −50 km. The aircraft measurements of vertical motion were not suitable for measuring weak vertical motion over large distances. Thus, it was necessary to use potential temperature data to estimate vertical parcel displacements and suggest the proper vertical interpolation of the wind observations.

The potential temperature data were used in several ways. First, the aircraft soundings at +20 km and −50 km were compared. It was found that the base of the northwestern sounding (at 1700 m) was 0.6°C warmer than the top of the southeastern sounding (at 1700 m). From the lapse rates of the two soundings, this suggests that the isentropes at the northwestern edge of the cross section are displaced 30 m to 100 m downward relative to isentropes at the southeastern edge. However, the large-scale temperature structure as deduced from the 1200 UTC 12 Dec soundings at Portland, ME, Albany, NY, and Chatham, MA suggests an expected *upward* displacement of 50 m. Thus, air parcels traveling from southeast to northwest within the warm front have experienced a net downward displacement of 80 m to 150 m relative to the larger-scale flow. Assuming from the 50 m large-scale isentropic slope an upward parcel displacement due to large-scale ascent of roughly 25 m, we conclude that the total vertical displacement is roughly −55 to −125 m for parcels within the warm front inversion traveling from southeast to northwest along the cross section.

A second measure of the vertical displacement of the warm front is given by the knowledge that because parcels within the marine layer accelerate northwestward as they pass over the coastal front, there must be a localized horizontal pressure gradient present to accelerate the air parcels. Assuming that this pressure gradient is obtained hydrostatically by the downward displacement of air above the marine layer, the magnitude of the necessary displacement can be calculated. The Bernoulli equation, when applied to a streamline that undergoes no vertical displacement (in this case, located at about 1200 m), indicates that a parcel ac-

celeration from 11 m s^{-1} to 15 m s^{-1} requires a pressure drop of 0.65 mb. If this pressure drop is produced hydrostatically entirely within the warm front, the warm front must undergo a net downward displacement of about 100 m. A downward displacement of similar magnitude is required for the more gradual acceleration observed in the marine layer well beyond the front. In reality, a significant fraction of the pressure drop is likely to be caused by downward displacement above the warm front, so we therefore expect a total vertical displacement of 100 m to 150 m, with about half of the displacement realized directly above the frontal updraft. The horizontal scale of the downward displacement above the frontal updraft is determined from aircraft observations of the horizontal scale of the acceleration.

The two techniques above suggest a net downward displacement within the warm front on the order of 100 m, with much of the displacement concentrated over the coastal front itself. This topography of the warm front inversion is consistent with the numerical simulation of Baines and Leonard (1989) for the case of subcritical flow flowing over a front-shaped obstacle. The vertical interpolation of winds above 700 m was, therefore, subjectively tuned to yield vertical streamline displacements of about 100 m within the warm front inversion.

REFERENCES

Baines, B. G., and B. P. Leonard, 1989: The effects of rotation on flow of a single layer over a ridge. *Quart. J. Roy. Meteor. Soc.*, **115,** 293–308.

Ball, F. K., 1960: A theory of fronts in relation to surface stress. *Quart. J. Roy. Meteor. Soc.*, **86,** 51–66.

Ballentine, R. J., 1980: A numerical investigation of New England coastal frontogenesis. *Mon. Wea. Rev.*, **108,** 1479–1497.

Bell, G. D., and L. F. Bosart, 1988: Appalachian cold-air damming. *Mon. Wea. Rev.*, **116,** 137–161.

Benjamin, T. B., 1968: Gravity currents and related phenomena. *J. Fluid Mech.*, **31,** 209–248.

Bond, N. A., and R. G. Fleagle, 1985: Structure of a cold front over the ocean. *Quart. J. Roy. Meteor. Soc.*, **111,** 739–759.

Bosart, L. F., 1975: New England coastal frontogenesis. *Quart. J. Roy. Meteor. Soc.*, **101,** 957–978.

——, 1981: The President's Day snowstorm of 18–19 February 1979: A subsynoptic-scale event. *Mon. Wea. Rev.*, **109,** 1542–1566.

——, C. J. Vaudo and J. H. Helsdon, Jr., 1972: Coastal frontogenesis. *J. Appl. Meteor.*, **11,** 1236–1258.

Britter, R. E., and J. E. Simpson, 1978: Experiments on the dynamics of a gravity current head. *J. Fluid Mech.*, **88,** 223–240.

Browning, K. A., and T. W. Harrold, 1970: Air motion and precipitation at a cold front. *Quart. J. Roy. Meteor. Soc.*, **96,** 369–389.

Brundidge, K. C., 1965: The wind and temperature structure of nocturnal cold fronts in the first 1420 feet. *Mon. Wea. Rev.*, **93,** 587–603.

Carbone, R. E., 1982: A severe frontal rainband. Part I: Stormwide hydrodynamic structure. *J. Atmos. Sci.*, **39,** 258–279.

Charba, J., 1974: Application of gravity current model to analysis of squall-line gust front. *Mon. Wea. Rev.*, **102,** 140–156.

Clarke, R. H., 1961: Mesostructure of dry cold fronts over featureless terrain. *J. Meteor.*, **18,** 715–735.

Droegemeier, K. K., and R. B. Wilhelmson, 1987: Numerical simulation of thunderstorm outflow dynamics. Part I: Outflow sensitivity experiments and turbulence dynamics. *J. Atmos. Sci.*, **44,** 1180–1210.

Forbes, G. S., R. A. Anthes and D. W. Thomson, 1987: Synoptic and mesoscale aspects of an Appalachian ice storm associated with cold-air damming. *Mon. Wea. Rev.*, **115,** 564–591.

Garner, S. T., 1986: An orographic mechanism for rapid frontogenesis. Ph.D. thesis, Massachusetts Institute of Technology, 222 pp.

Garratt, J. R., and W. L. Physick, 1986: Numerical study of atmospheric gravity currents. Part I: Simulations and observations of cold fronts. *Beitr. Phys. Atmos.*, **59,** 283–300.

George, J. J., 1960: *Weather Forecasting for Aeronautics.* Academic Press, 673 pp.

Goff, R. C., 1976: Vertical structure of thunderstorm outflows. *Mon. Wea. Rev.*, **104,** 1429–1440.

Hobbs, P. V., and P. O. G. Persson, 1982: The mesoscale and microscale structure and organization of clouds and precipitation in midlatitude cyclones. Part V: The substructure of narrow cold-frontal rainbands. *J. Atmos. Sci.*, **39,** 280–295.

Jirka, G. H., and M. Arita, 1987: Density currents or density wedges: Boundary-layer influence and control methods. *J. Fluid Mech.*, **177,** 187–206.

Lawson, T. J., 1971: Haboob structure at Khartoum. *Weather,* **26,** 105–112.

Locatelli, J. D., and P. V. Hobbs, 1974: Fall speeds and masses of solid precipitation particles. *J. Geophys. Res.*, **79,** 2185–2197.

Marks, F. D., Jr., and P. M. Austin, 1979: Effects of the New England coastal front on the distribution of precipitation. *Mon. Wea. Rev.*, **107,** 53–67.

McCarthy, D. H., 1977: A study of the vertical structure of the New England coastal front. M.S. thesis, Univ. of Wisconsin, Madison, 82 pp.

Miles, J. W., and L. N. Howard, 1964: Note on a heterogeneous shear flow. *J. Fluid Mech.*, **20,** 331–336.

Mitchell, K. E., and J. B. Hovermale, 1977: A numerical investigation of the severe thunderstorm gust front. *Mon. Wea. Rev.*, **105,** 657–675.

Nielsen, J. W., 1989: The formation of New England coastal fronts. *Mon. Wea. Rev.*, **117,** 1380–1401.

Riordan, A. J., S. SethuRaman, J. M. Davis and S. Viessman, 1985: Measurements in the marine boundary layer near a coastal front. *Geophys. Res. Lett.*, **12,** 681–684.

Sanders, F., 1983: Observations of fronts. *Mesoscale Meteorology—Theories, Observations, and Methods.* D. K. Lilly, T. Gal-Chen, Eds., D. Reidel, 175–203.

SethuRaman, and A. J. Riordan, 1988: The Genesis of Atlantic Lows Experiment: The planetary-boundary-layer subprogram of GALE. *Bull. Amer. Meteor. Soc.*, **69,** 161–172.

Shapiro, M. A., 1984: Meteorological tower measurements of a surface cold front. *Mon. Wea. Rev.*, **112,** 1634–1649.

——, T. Hampel, D. Rotzoll and F. Mosher, 1985: The frontal hydraulic head: A micro-α scale ($\sim$1 km) triggering mechanism for mesoconvective weather systems. *Mon. Wea. Rev.*, **113,** 1166–1183.

Simpson, J. E., 1969: A comparison between laboratory and atmospheric density currents. *Quart. J. Roy. Meteor. Soc.*, **95,** 758–765.

——, 1982: Gravity currents in the laboratory, atmosphere and ocean. *Ann. Rev. Fluid Mech.*, **14,** 213–234.

——, 1987: *Gravity Currents: In the Environment and the Laboratory.* John Wiley and Sons, 244 pp.

——, and R. E. Britter, 1980: A laboratory model of an atmospheric mesofront. *Quart. J. Roy. Meteor. Soc.*, **106,** 485–500.

——, D. A. Mansfield and J. R. Milford, 1977: Inland penetration of sea-breeze fronts. *Quart. J. Roy. Meteor. Soc.*, **103,** 47–76.

Smith, R. K., and M. J. Reeder, 1988: On the movement of low-level structure of cold fronts. *Mon. Wea. Rev.*, **116,** 1927–1944.

Thorpe, S. A., 1973: Experiments on instability and turbulence in a stratified shear flow. *J. Fluid Mech.*, **61,** 731–751.

Wakimoto, R. M., 1982: The life cycle of thunderstorm gustfronts as viewed with Doppler radar and rawinsonde data. *Mon. Wea. Rev.*, **110,** 1060–1082.

Young, G. S., and R. H. Johnson, 1984: Meso- and microscale features of a Colorado cold front. *J. Climate Appl. Meteor.*, **23,** 1315–1325.